Label-free *in vivo* flow cytometry in zebrafish using two-photon autofluorescence imaging

Yan Zeng,[1] Jin Xu,[2] Dong Li,[1] Li Li,[2] Zilong Wen,[2] and Jianan Y. Qu[1,*]

[1]*Department of Electronic and Computer Engineering, Hong Kong University of Science and Technology, Clear Water Bay, Kowloon, Hong Kong, China*

[2]*State Key Laboratory of Molecular Neuroscience, Department of Biochemistry, Hong Kong University of Science and Technology, Clear Water Bay, Kowloon, Hong Kong, China*

**Corresponding author: eequ@ust.hk*

Received February 13, 2012; revised April 9, 2012; accepted May 7, 2012; posted May 10, 2012 (Doc. ID 162946); published June 20, 2012

We demonstrate a label-free *in vivo* flow cytometry in zebrafish blood vessels based on two-photon excited autofluorescence imaging. The major discovery in this work is the strong autofluorescence emission from the plasma in zebrafish blood. The plasma autofluorescence provides excellent contrast for visualizing blood vessels and counting blood cells. In addition, the cellular nicotinamide adenine dinucleotide autofluorescence enables *in vivo* imaging and counting of white blood cells (neutrophils). © 2012 Optical Society of America

OCIS codes: 170.1470, 170.3880, 180.4315, 180.5810, 170.6935.

Monitoring blood rheology (hemorheology) and imaging various circulating cells in the blood flow are crucial for early diagnosis, prognosis, and prevention of disease development, and for biomedical study of disease evolution, for instance, cardiovascular disorder, stroke, sickle cell anemia, infection, leukemia, and cancer metastasis [1]. Conventionally, drawing blood is an indispensable process to characterize blood with a hemocytometer or flow cytometry. The procedures lack capability to continuously monitor the biological dynamics within blood flow in a native biological environment. The recent advances of *in vivo* flow cytometry provide opportunities to detect and image various types of cells in blood and lymph flows [1]. Using confocal and two-photon systems equipped with fluorescence labeling techniques, noninvasive detection of red blood cells (RBCs), white blood cells (WBCs) and circulating tumor cells (CTCs) in the circulation system have been successfully demonstrated [2,3]. However, the potential cytotoxicity induced by fluorescent labels is highly concerning [4]. Without sample preparation and potential cytotoxicity, a label-free technology providing morphological and biochemical information is highly desirable [4].

The integrated photothermal (PT) and photoacoustic (PA) platforms have been developed for *in vivo* differentiation of blood cells using intrinsic absorbers (hemoglobin in RBCs, cytochrome in WBCs, and melanin in CTCs) [1]. The PT method is currently able to work in the transillumination mode. The imaging of opaque tissue becomes challenging. The PA-based technology indeed provides excellent blood flow detection, microvascular imaging, and oxygen saturation characterization [5], but it encounters difficulties in label-free detection of WBCs and in achieving individual cell imaging or counting in the blood flow. In a previous study, we demonstrated that with well-known and newly discovered endogenous fluorophores, such as nicotinamide adenine dinucleotide (NADH), tryptophan, and hemoglobin, the two-photon excited autofluorescence provides good contrast for potential imaging of various blood cells noninvasively [6,7]. In this study, we develop a new *in vivo* flow cytometry using two-photon excited fluorescence (TPEF) imaging to visualize blood flow and count individual RBCs and WBCs in zebrafish, a promising animal model for studying various human diseases [8]. The strong autofluorescence emission from plasma discovered in this study is used to provide negative contrast for visualizing RBCs while the NADH signals in WBCs enable imaging and counting of WBCs. Moreover, the blood flow images provide the information to quantify blood rheological properties.

A TPEF spectroscopic imaging system was modified from that reported in our previous work [6]. Briefly, the excitation sources were generated from a tunable femtosecond Ti:sapphire laser (720–800 nm) and a supercontinuum from a photonic crystal fiber (PCF) pumped by the femtosecond laser. The excitations at 600 ± 20 and 650 ± 22 nm were filtered out from the supercontinuum using two interference filters, respectively. A water immersion objective lens (40×, 1.1 NA, Zeiss) of 500 μm working distance was used to focus the excitation beam. To avoid tissue damage, the excitation power was kept not over 15 mW. The TPEF signals were conducted to a spectrograph equipped with a 16-photomultiplier tube array and a time-correlated single photon counting (TCSPC) module (PML-16-C-0 and SPC-150, Becker & Hickl). To form a regular TPEF image at a certain depth, a pair of galvo mirrors was applied to create a sampling area of 90×90 μm^2. The imaging depth was determined by an actuator. For the mode of live cell imaging and counting in the blood flow, the excitation focal point was scanned perpendicularly across the blood vessels using one of the galvo mirrors. The scanning along the blood vessel was passively achieved by the blood flow itself. The detection system for both imaging modes recorded the signals of each pixel in time and spectral domains. The zebrafish was cultured following the standard procedure [9]. Fish embryos of 2 to 3 days post fertilization (dpf) were anesthetized with 0.02% tricaine, and over 20 embryos were examined by our imaging system. This study was approved by the University Animal Care Committee.

The wide-field transmission image of a zebrafish is shown in Fig. 1(a). Two major circulation vessels (dorsal aorta and axial vein) can be observed [bottom in

Fig. 1(a)]. In order to identify the blood vessels with TPEF signals, we used a Tg (*gata1*: DsRed) transgenic zebrafish of RBCs expressed with red fluorescent protein (DsRed) in the study. The excitation wavelength was first set at 720 nm for effective excitation of DsRed due to two-photon resonance absorption. The representative TPEF images formed with the signals recorded in the wavelength band from 400 to 540 nm, the typical band of tissue autofluorescence, and the wavelength band from 550 to 600 nm, the band of DsRed fluorescence, are shown in Figs. 1(b) and 1(c), respectively. The image in Fig. 1(c) clearly shows the parallel aorta and vein with the signals from DsRed-marked RBCs. The shapes of RBCs were significantly distorted into bright lines because the scanning speed of the galvo mirrors was relatively slow in the regular x-y scanning imaging mode. Because Figs. 1(b) and 1(c) were recorded simultaneously, the aorta and vein in Fig. 1(b) could be defined by using DsRed signals in Fig. 1(c). Strong autofluorescence emission was found from the plasma in blood vessels as shown in Fig. 1(b). To study the spectral characteristics of plasma autofluorescence, we integrated signals from all the pixels from the blood vessels. The integrated spectral signals are shown in Fig. 1(d). The strong TPEF signals from plasma are well separated from the DsRed signals from RBCs.

To further understand the plasma TPEF signals, we utilized different excitation at 600, 650, 720, 760, and 800 nm to study their spectral characteristics. The results are shown in Fig. 1(e). The TPEF signals at 600 and 650 nm excitations are almost identical, and their fluorescence peak is located around 405 nm. The hemoglobin fluorescence peak around 440 nm was found very weak in the RBCs of zebrafish. With the excitation wavelength above 700 nm, the plasma fluorescence peaks redshift with the increase of excitation wavelength as shown in Fig. 1(e), while the excitation efficiency drops rapidly (data not shown). The excitation and emission characteristics of plasma autofluorescence have certain similarity to the large fluorescent molecules of complex energy states such as collagen and elastin. Though the origin of the plasma autofluorescence is still unknown, the results indicate that the autofluorescence in plasma could be used as an endogenous source to provide contrast for imaging blood flow and blood cells in the zebrafish model. In addition, the discovery should be valuable to biochemical exploration for the development of new biocompatible fluorescent labels. It should be pointed out that we did not observe the similar plasma autofluorescence from the blood samples freshly extracted from mice and humans.

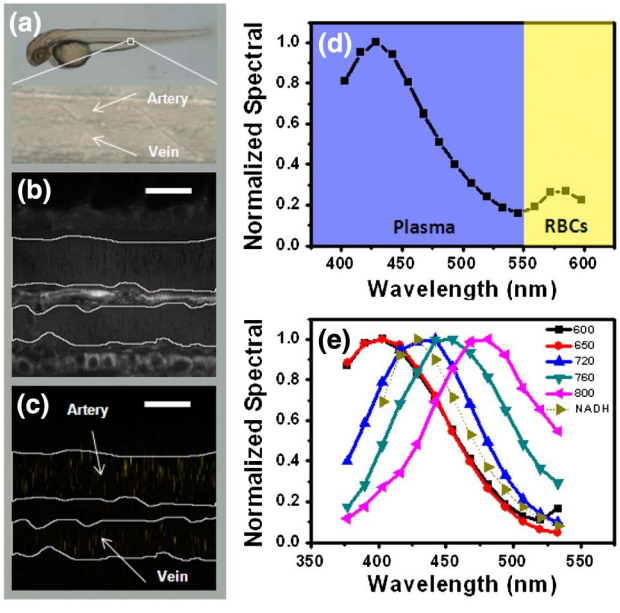

Fig. 1. (Color online) Fluorescence characteristics of plasma in zebrafish. (a) Wide-field images of zebrafish and zebrafish blood vessels; (b) and (c) TPEF images formed with the signals in 400–540 nm and 550–600 nm bands ($\lambda_{ex} = 720$ nm), respectively; (d) TPEF spectral signals extracted from the regions of dorsal aorta and axial vein marked in (b) and (c); (e) spectra of the plasma TPEF signals at 600, 650, 720, 760, and 800 nm excitation and the NADH fluorescence extracted from surrounding tissue. Scale bars in (b) and (c): 20 μm.

To demonstrate the label-free *in vivo* flow cytometry using the intrinsic fluorescence signals, we firstly chose 650 nm as an excitation source because the plasma autofluorescence at 650 nm excitation is peaked at 405 nm, well separated from the cell/tissue autofluorescence dominated by the NADH signal that is peaked at 440 nm as shown in Fig. 1(e) [10]. The spectral difference can be used to differentiate the plasma from WBCs in the blood stream and the endothelial cells on the blood vessel walls. In the mode of cell imaging and counting, we scanned the focal point across the vessels rapidly at 200 Hz and used the blood flow itself to create scanning along the examined blood vessel. A typical time-lapsed image of blood flow in a vein is shown in Fig. 2(a), and the negative images of RBCs (dark spots) can be clearly identified over the bright background of the plasma autofluorescence. Though the RBC shape is distorted, the image size of RBCs is relatively uniform, indicating that the blood flow in the vein is almost constant. Therefore, the blood flow image from the vein should provide valuable information to quantify rheological properties of blood flow such as hematocrit, RBC counts, RBC deformability, and aggregation, which are crucial in the progression of many diseases [11].

The other important modality of a flow cytometry is to differentiate blood cell types. Figures 2(b) and 2(c) show the images of blood flow in axial vein measured from a Tg (*lyz*: DsRed) transgenic zebrafish with its neutrophils marked by DsRed. The purpose in using the transgenic zebrafish is to verify how accurately the individual RBCs and neutrophils in the blood stream can be detected using plasma and NADH fluorescence, respectively. The image displayed in Fig. 2(b) was formed with the TPEF signals recorded in the DsRed fluorescence band of 520–559 nm, and the image in Fig. 2(c) was formed with the signals in the band of 364–507 nm, in which the signals in the bands of 364–416 nm and 429–507 nm are coded with red and cyan color, respectively. The blood flow image in Figs. 2(b) and 2(c) allowed us to identify the pixels of neutrophil and plasma. The extracted TPEF spectral signals are shown in Fig. 2(d). The comparison of the spectral signal of neutrophil with the zebrafish tissues shows that they are almost identical and are dominated by the NADH signals peaked at 440 nm. The difference in TPEF spectral lineshape

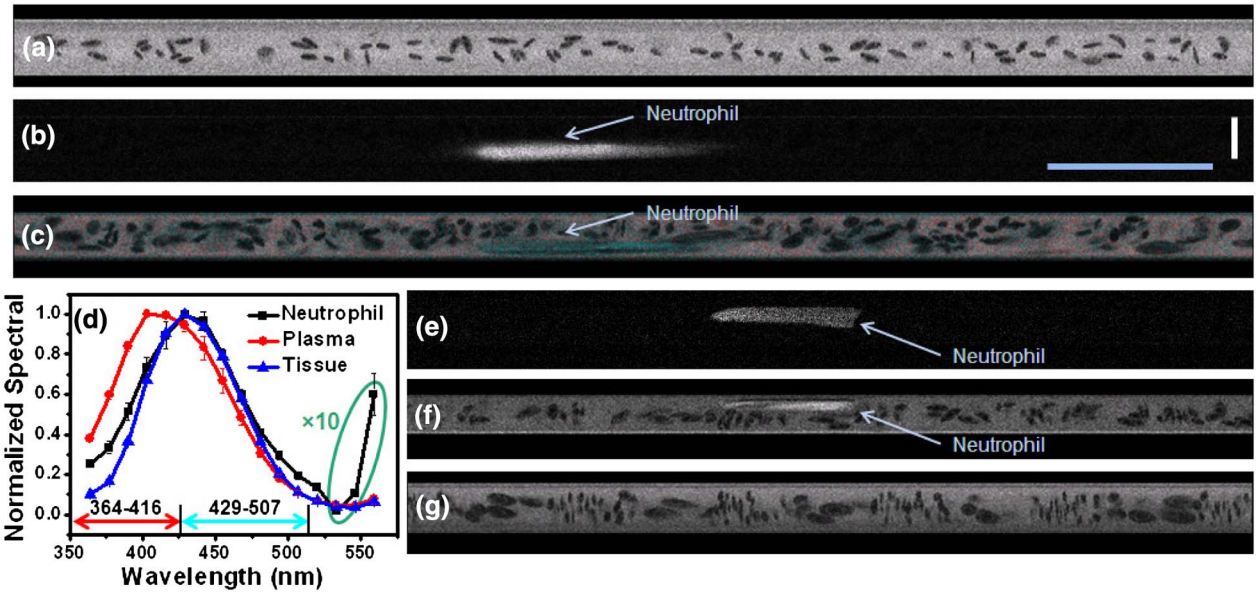

Fig. 2. (Color online) Blood flow images of Tg (*lyz*: DsRed) transgenic zebrafish. (a) Blood flow image of axial vein in zebrafish at 650 nm excitation; (b) and (c) blood flow images formed with the signals in 550–600 nm and 400–540 nm bands at 650 nm excitation; (d) fluorescence spectral signals extracted from neutrophil, plasma and tissue; (e) and (f) blood flow images formed with DsRed signals and the signals below 550 nm at 720 nm excitation; (g) blood flow image of dorsal aorta in zebrafish at 720 nm excitation. Scale bars for all flow images are shown in (b): vertical (spatial scale), 25 μm; horizontal (temporal scale), 1 s.

between neutrophil and plasma provides a contrast to differentiate them from each other as shown in the color-coded image in Fig. 2(c). The neutrophil was found attached to the vessel wall, and its image had a long tail. This is consistent with the well-known phenomena that the neutrophil rolls along the vessel wall and moves more slowly than RBCs [12]. Moreover, the color-coded blood flow image also clearly differentiates the plasma from the blood vessel walls featured by a line of endothelial cells with autofluorescence dominated by NADH signals as shown in Fig. 2(c). Finally, it should be pointed out that we found numerous small-sized spots of the NADH-like fluorescence signal with intensity comparable to neutrophil and plasma. They could be the emission from small blood cells, such as thrombocytes of size from 2 to 3 μm.

Though NADH and plasma fluorescence excited at 650 nm can differentiate neutrophils from plasma, the excitation source was the supercontinuum from a PCF pumped by a standard Ti:sapphire laser. Figures 2(e) and 2(f) show the blood flow images formed by the DsRed signal band and the signals below 550 nm with the excitation of a Ti:sapphire laser tuned at 720 nm. As can be seen, neutrophil still can be differentiated from plasma and RBCs because of the high excitation efficiency of NADH at 720 nm excitation [13] and relatively low excitation efficiency of plasma fluorescence compared with 600 and 650 nm excitation. Moreover, Figs. 2(f) and 2(g) display the difference in RBC patterns between the blood flow images of vein and aorta. The images of RBCs in the dorsal aorta show great irregularity, showing that individual RBC images expanded during the diastole because of slow blood flow while the compressed pattern of RBCs was observed during systole due to faster blood flow. The group pattern of RBCs was repeated periodically and synchronized with the heartbeat of the zebrafish. Quantitatively, the RBC counting rates are 10.4, 16, 14.5, and 23 per sec in Figs. 2(a), 2(c), 2(f), and 2(g), respectively. The maximum counting rates should be dependent on the scanning speed of the galvo mirror and excitation power. For the measurement of large-sized embryos or fish, the issue of optical penetration can be solved by imaging the blood vessels close to the surface or fish tail where the thickness of tissue above the imaged blood vessels is similar to the fish embryos of 2–3 dpf.

This work was supported by the Hong Kong Research Grants Council through grants 662711, N_HKUST631/11 and T13-706/11-1, and HKUST through grant RPC10EG33.

References

1. V. V. Tuchin, A. Tárnok, and V. P. Zharov, Cytom. A **79**, 737 (2011).
2. J. Novak, I. Georgakoudi, X. Wei, A. Prossin, and C. P. Lin, Opt. Lett. **29**, 77 (2004).
3. C. F. Zhong, E. R. Tkaczyk, T. Thomas, J. Y. Ye, A. Myc, A. U. Bielinska, Z. Cao, I. Majoros, B. Keszler, J. R. Baker, and T. B. Norris, J. Biomed. Opt. **13**, 034008 (2008).
4. G. A. Wagnières, W. M. Star, and B. C. Wilson, Photochem. Photobiol. **68**, 603 (1998).
5. L. V. Wang, Nat. Photon. **3**, 503 (2009).
6. W. Zheng, D. Li, Y. Zeng, Y. Luo, and J. Y. Qu, Biomed. Opt. Express **2**, 71 (2011).
7. D. Li, W. Zheng, and J. Y. Qu, Opt. Lett. **34**, 2853 (2009).
8. G. J. Lieschke and P. D. Currie, Nat. Rev. Genet. **8**, 353 (2007).
9. D. F. Edwards, *The Zebrafish Book: A Guide for the Laboratory Use of Zebrafish (Danio rerio)*, 3rd ed. (University of Oregon, 1995).
10. W. Zheng, Y. Wu, D. Li, and J. Y. Qu, J. Biomed. Opt. **13**, 054010 (2008).
11. E. I. Galanzha and V. P. Zharov, Cytom. A **79**, 746 (2011).
12. K. Ley, C. Laudanna, M. I. Cybulsky, and S. Nourshargh, Nat. Rev. Immunol. **7**, 678 (2007).
13. W. R. Zipfel, R. M. Williams, R. Christiet, A. Y. Nikitin, B. T. Hyman, and W. W. Webb, Proc. Natl. Acad. Sci. USA **100**, 7075 (2003).